FURTHER REFINEMENT OF THE NONPLANAR ASPECTS OF THE SUBSONIC DOUBLET–LATTICE LIFTING SURFACE METHOD

William P. Rodden*
William P. Rodden, Ph.D., Inc.
La Cañada Flintridge, California 91011-2838, USA

Paul F. Taylor**
Gulfstream Aerospace Corporation
Savannah, Georgia 31402, USA

and

Samuel C. McIntosh, Jr.†
McIntosh Structural Dynamics
Mountain View, California 94040, USA

ABSTRACT

The Doublet–Lattice Method (DLM) is in use world–wide for flutter and dynamic response analyses of aircraft at subsonic speeds. The existing method is based on the paper "Refinement of the Nonplanar Aspects of the Subsonic Doublet–Lattice Lifting Surface Method" by Rodden, Giesing, and Kalman. The present paper develops a further refinement to extend its frequency limits for applications to higher frequency flutter (e.g. for aeroservoelastic systems with high frequency control surfaces) and dynamic response (e.g. for short wavelength gusts).

The DLM is an aerodynamic finite element method for modeling oscillating interfering lifting surfaces in subsonic flows. It reduces to the Vortex–Lattice Method (VLM) at zero reduced frequency. The number of finite elements ("boxes") required for accurate results depends on aspect ratio and reduced frequency, among other parameters. At high reduced frequency, the chordwise dimension of the boxes must be small. However, an approximation in the method, viz., that the variation of the numerator of the incremental oscillatory kernel function is parabolic across the span of the box bound vortex, restricts the box aspect ratio to about 3. Hence, high frequency requirements bring an associated requirement for a large number of boxes in the aerodynamic idealization.

If a higher order approximation is used for the spanwise variation of the numerator of the incremental oscillatory kernel, the limitation on box aspect ratio can be relaxed and the number of spanwise divisions required in high frequency analyses will be reduced significantly, leading to a reduction in the total number of boxes.

This paper replaces the original parabolic approximation by a quartic approximation‡. The quartic curve fitting coefficients are determined for the planar and nonplanar kernels, and the new integrals for the planar and nonplanar normalwash factors are evaluated. The refinement is incorporated into a DLM code previously known as N5KA, and convergence studies on typical configurations are presented that attempt to specify a higher limit for practical box aspect ratios.

* Consulting Engineer
** Loads and Dynamics Engineer
† Consulting Engineer
‡ The analytical development was performed while the first author was Visiting Professor of Aerospace Engineering at the Technion - Israel Institute of Technology, Haifa, Israel, during April-June 1995.

NOMENCLATURE

A, B, C, D, E	coefficients in quartic approximations to kernel numerators; subscripts 1 and 2 refer to planar and nonplanar parts of kernel, respectively
b_r	reference semichord
C_L	total lift coefficient
D_{rs}	normalwash factor; D_{0rs} is steady normalwash factor; D_{1rs} and D_{2rs} are incremental oscillatory planar and nonplanar normalwash factors, respectively
e	box semiwidth
F	integral in Eq. (21)
K	kernel function; K_1 and K_2 are factors in numerators of planar and nonplanar parts of kernel, respectively
k_r	reference reduced frequency, $k_r = \omega b_r/U$
M	Mach number
N	number of lifting surfaces
p	lifting pressure coefficient
$Q(\bar{\eta})$	quartic approximation to kernel numerator; Q_1 and Q_2 are approximations for planar and nonplanar numerators, respectively
r	cylindrical radius from sending doublet
S_n	area of nth lifting surface
s	semispan
T	direction cosine function; T_1 and T_2^* are functions for planar and nonplanar parts of kernel, respectively
U	freestream velocity
w	dimensionless normalwash

x_0, y_0, z_0 Cartesian coordinates of receiving point relative to midpoint of sending line (bound vortex)

$\bar{x}$ Streamwise distance between an arbitrary point on the sending line and the receiving point

$\bar{y}, \bar{z}$ Coordinates of receiving point relative to midpoint of sending line parallel and perpendicular to sending box

ε parameter defined in Eq. (24)

γ dihedral angle; γ_r and γ_s are dihedral angles of receiving and sending boxes, respectively, and $\bar{\gamma}_r = \gamma_r - \gamma_s$ is the relative dihedral angle between receiving and sending boxes

Δx_s centerline chord of sending box

$\bar{\eta}$ spanwise coordinate, in the plane of an element

λ_s sweepback angle of sending box 1/4–chord line

ω circular frequency

Note: Additional nomenclature is defined in the appendices.

INTRODUCTION

The Doublet–Lattice Method (DLM)[1] is a finite–element method for the solution of the oscillatory subsonic pressure–normalwash integral equation for multiple interfering surfaces

$$w(x,s)=(1/8\pi)\sum_{n=1}^{N}\int\int_{s_n} K(x,\xi;s,\sigma)p(\xi,\sigma)d\xi d\sigma \qquad (1)$$

where w is the complex amplitude of the dimensionless normalwash, p is the complex amplitude of the lifting pressure coefficient, (x,s) are the orthogonal coordinates on the nth surface S_n such that the undisturbed stream is parallel to the x–axis, and K is the complex acceleration potential kernel for oscillatory subsonic flow. The original DLM algorithm was presented at the same time (1968) as the Lifting Line Element Method (LLEM) of Stark[2]. Although numerous comparisons[2,3] with experiments were shown at the time, the complete details of the LLEM were never published. Dr. Stark has written a note on the LLEM, and this is included here as Appendix A.

A refinement to the expressions for the kernel given by Rodemich[4] and Landahl[5] was presented by Rodden, Giesing and Kalman[6] in the form

$$K = (K_1 T_1/r^2 + K_2 T_2^*/r^4)\exp(-i\omega\bar{x}/U) \qquad (2)$$

in order to analyze the nonplanar interference correctly. K_1 and K_2 are the planar and nonplanar parts of the kernel numerator, respectively. Here ω is the frequency, x_0 is the distance between the sending and receiving points parallel to the freestream, U is the velocity of the freestream,

$$T_1 = \cos(\gamma_r - \gamma_s) \qquad (3)$$

$$T_2^* = (z_0\cos\gamma_r - y_0\sin\gamma_r)(z_0\cos\gamma_s - y_0\sin\gamma_s) \qquad (4)$$

$$r^2 = z_0^2 + y_0^2 \qquad (5)$$

where y_0 and z_0 are the Cartesian distances between sending and receiving points perpendicular to the freestream, and γ_r and γ_s are the dihedral angles at the receiving and sending points, respectively. The coordinate system is illustrated in Fig. 1. The description of K_1 and K_2 as the planar and nonplanar parts of the kernel numerator is a convenience because both are obviously nonplanar in general. The refinement in Eq. (2) is in the second term; this was found necessary so that the DLM could predict the interference between a *nearly planar* wing and horizontal tail[6]. The refinement retained the original primary approximation[1], i.e., that the *incremental* oscillatory normalwash factors are obtained by integrating the difference between the oscillatory and steady kernels over the length of the bound vortex assuming a quadratic (parabolic) variation in the numerator of the difference. The total normalwash factor is then the sum of the incremental oscillatory normalwash factor and the steady normalwash factor obtained from the expressions for a horseshoe vortex, e.g., the Vortex–Lattice Method (VLM) of Hedman[7]. In this way, the DLM converges to the VLM at zero reduced frequency, and the error in the parabolic approximation of the kernel numerator difference is small at low reduced frequencies and increases with the reduced frequency.

Extensive experience with the VLM and DLM has led to guidelines for idealization of lifting surfaces into finite element models. It is assumed that each surface can be approximated by segments of planes. The surface is divided into small trapezoidal panels ("boxes") in a manner such that the boxes are arranged in strips parallel to the freestream (Fig. 2) and surface edges and fold lines lie on box boundaries. Boxes should be concentrated near wing edges and hinge lines or any other place where downwash is discontinuous and pressures have large gradients. (The usual practice is not to concentrate boxes near hinge lines because viscous effects, which dominate trailing edge control surface aerodynamics, reduce hinge moments from potential theory results, so more chordwise boxes tend to over-predict hinge moments). The chord lengths of adjacent boxes in the streamwise direction should only change gradually. If a surface lies in (or nearly in) the plane of another surface, the spanwise divisions of the downstream surface should lie along the spanwise divisions of the upstream surface. Strips at the intersection of lifting surfaces should have approximately equal widths.

The foregoing qualitative modeling recommendations have been quantified [the guidelines have been summarized by Rodden and Johnson[8]] as follows. The aspect ratio of the boxes should be less than three. The chord length of the box-

es should be less than 0.08 times the minimum velocity divided by the maximum frequency (in Hz) of interest, i.e., $\Delta x < 0.08U/f$ (Note: this is a requirement for approximately 12 boxes per minimum wave length; however, no less than four boxes per chord should be used). The limitation of box aspect ratio to three is a consequence of the DLM assumption of a parabolic variation in the incremental kernel numerator. The variation of the real part of the incremental kernel numerator along the box quarter-chord is shown in Figure 3 for an aspect ratio of 1.

Aeroservoelastic analyses frequently deal with high frequencies in control system components, and new design criteria for short wavelength gusts (e.g., the FAA[9] and JAA[10] tuned discrete gust require a minimum gradient distance of 30 feet be analyzed) also require that higher reduced frequencies be considered. The combination of the box chord length limitation and the box aspect ratio limitation can result in a requirement for a large number of aerodynamic boxes. A higher order (than quadratic) approximation to the numerator of the incremental oscillatory kernel will increase the limit on box aspect ratio for accurate oscillatory aerodynamic analysis. This paper considers a further refinement to the DLM in a quartic approximation and then attempts to determine a new practical limit on maximum box aspect ratio.

NEW REFINEMENT

The original method for determining the influence of an oscillating lifting surface element at a point was based on the assumption that the lifting pressure could be concentrated along a line. The line is located at the 1/4–chord line of the element (Fig. 2). The lifting load line is represented by a horseshoe vortex for its steady effects and a line of doublets for its incremental oscillatory effects. The surface boundary condition is a prescribed normalwash at the control point of each box which is located at the 3/4–chord point along the centerline of each box. The numerical form of the integral equation, Eq. (1), in matrix notation becomes

$$\{w\} = [D]\{p\} \tag{6}$$

where the elements of the normalwash factor matrix $[D]$ are

$$D_{rs} = (\Delta x_s/8\pi)\int_{-e}^{+e} K\, d\bar{\eta} \tag{7}$$

Here Δx_s is the centerline chord of the sending box, e is its semiwidth, and the streamwise integration of the kernel has been performed by concentrating the lifting pressure at the 1/4–chord load line.

The evaluation of the normalwash factor Eq. (7) in element coordinates gives

$$D_{rs} = (\Delta x_s/8\pi)\int_{-e}^{+e}(K_1T_1/r^2 + K_2T_2^*/r^4)\mathrm{x} \exp[-i\omega(x_0-\bar{\eta}\tan\lambda_s)/U]d\bar{\eta} \tag{8}$$

where $r^2 = (\bar{y}-\bar{\eta})^2 + \bar{z}^2$ and λ_s is the sweep of the 1/4-chord line of the sending box. The normalwash factor is evaluated as before by adding and subtracting the steady values of K_1 and K_2, denoted by K_{10} and K_{20}, respectively, from their oscillatory counterparts. Then, Eq. (8) becomes

$$D_{rs} = D_{0rs} + D_{1rs} + D_{2rs} \tag{9}$$

where

$$D_{0rs} = \frac{\Delta x_s}{8\pi}\int_{-e}^{+e}\left[\frac{K_{10}T_1}{r^2} + \frac{K_{20}T_2^*}{r^4}\right]d\bar{\eta} \tag{10}$$

$$D_{1rs} = \frac{\Delta x_s}{8\pi}\int_{-e}^{+e}\frac{\{K_1\exp[-i\omega(x_0-\bar{\eta}\tan\lambda_s)/U]-K_{10}\}T_1}{r^2}d\bar{\eta} \tag{11}$$

$$D_{2rs} = \frac{\Delta x_s}{8\pi}\int_{-e}^{+e}\frac{\{K_2\exp[-i\omega(x_0-\bar{\eta}\tan\lambda_s)/U]-K_{20}\}T_2^*}{r^4}d\bar{\eta} \tag{12}$$

Eq. (10) is the steady normalwash factor and is more conveniently derived from horseshoe vortex considerations than by evaluating the integral. The steady downwash factor has been given by Hedman[7]. We may evaluate the incremental oscillatory normalwash factors [Eqs. (11) and (12)] in closed form by now approximating the numerators as quartics in $\bar{\eta}$. We rewrite Eq. (11) as

$$D_{1rs} = \frac{\Delta x_s}{8\pi}\int_{-e}^{+e}\frac{Q_1(\bar{\eta})}{(\bar{y}-\bar{\eta})^2+\bar{z}^2}d\bar{\eta} \tag{13}$$

where $Q_1(\bar{\eta})$ is the quartic approximation

$$\begin{aligned} Q_1(\bar{\eta}) &= A_1\bar{\eta}^2 + B_1\bar{\eta} + C_1 + D_1\bar{\eta}^3 + E_1\bar{\eta}^4 \\ &\approx \{K_1\exp[-i\omega(x_0-\bar{\eta}\tan\lambda_s)/U]-K_{10}\}T_1 \end{aligned} \tag{14}$$

If we denote the inboard, inboard intermediate, center, outboard intermediate, and outboard values of $Q_1(\bar{\eta})$ respectively by $Q_1(-e)$, $Q_1(-e/2)$, $Q_1(0)$, $Q_1(e/2)$ and $Q_1(e)$, the quartic coefficients are

$$A_1 = -\frac{1}{6e^2}[Q_1(-e) - 16Q_1(-e/2) + 30Q_1(0) - 16Q_1(e/2) + Q_1(e)] \tag{15}$$

$$B_1 = \frac{1}{6e}[Q_1(-e) - 8Q_1(-e/2) + 8Q_1(e/2) - Q_1(e)] \tag{16}$$

$$C_1 = Q_1(0) \tag{17}$$

$$D_1 = -\frac{2}{3e^3}[Q_1(-e) - 2Q_1(-e/2) + 2Q_1(e/2) - Q_1(e)] \tag{18}$$

$$E_1 = \frac{2}{3e^4}[Q_1(-e) - 4Q_1(-e/2) + 6Q_1(0) - 4Q_1(e/2) + Q_1(e)] \tag{19}$$

Then the planar downwash factor becomes

$$D_{1rs} = \frac{\Delta x_s}{8\pi}\Big\{[(\bar{y}^2 - \bar{z}^2)A_1 + \bar{y}B_1 + C_1 + \bar{y}(\bar{y}^2 - 3\bar{z}^2)D_1 + (\bar{y}^4 - 6\bar{y}^2\bar{z}^2 + \bar{z}^4)E_1]F + \Big[\bar{y}A_1 + \frac{1}{2}B_1 + \frac{1}{2}(3\bar{y}^2 - \bar{z}^2)D_1 + 2\bar{y}(\bar{y}^2 - \bar{z}^2)E_1\Big]\log\frac{(\bar{y}-e)^2 + \bar{z}^2}{(\bar{y}+e)^2 + \bar{z}^2} + 2e\Big[A_1 + 2\bar{y}D_1 + \Big(3\bar{y}^2 - \bar{z}^2 + \frac{1}{3}e^2\Big)E_1\Big]\Big\} \tag{20}$$

where the integral

$$F = \int_{-e}^{+e}\frac{d\bar{\eta}}{(\bar{y}-\bar{\eta})^2 + \bar{z}^2} = \frac{1}{|\bar{z}|}\operatorname{atan}\Big(\frac{2e|\bar{z}|}{\bar{y}^2 + \bar{z}^2 - e^2}\Big) \tag{21}$$

is evaluated as before[6]. The integral F may be rewritten as

$$F = \delta_1\frac{2e}{\bar{y}^2 + \bar{z}^2 - e^2}\Big(1 - \varepsilon\frac{\bar{z}^2}{e^2}\Big) + \delta_2\frac{\pi}{|\bar{z}|} \tag{22}$$

where

$$\delta_1 = 1, \delta_2 = 0 \text{ for } \bar{y}^2 + \bar{z}^2 - e^2 > 0$$
$$\delta_1 = 1, \delta_2 = \frac{1}{2} \text{ for } \bar{y}^2 + \bar{z}^2 - e^2 = 0 \tag{23}$$
$$\delta_1 = 1, \delta_2 = 1 \text{ for } \bar{y}^2 + \bar{z}^2 - e^2 < 0$$

in order to place the arctangent in the correct quadrant, and

$$\varepsilon = \frac{e^2}{\bar{z}^2}\Big[1 - \frac{\bar{y}^2 + \bar{z}^2 - e^2}{2e|\bar{z}|}\operatorname{atan}\Big(\frac{2e|\bar{z}|}{\bar{y}^2 + \bar{z}^2 - e^2}\Big)\Big] \tag{24}$$

When $\left|2e\bar{z}/(\bar{y}^2 + \bar{z}^2 - e^2)\right| \le 0.3$, the series expansion

$$\varepsilon = \frac{4e^4}{(\bar{y}^2 + \bar{z}^2 - e^2)^2}\sum_{n=2}^{7}\frac{(-1)^n}{2n-1}\Big(\frac{2e|\bar{z}|}{\bar{y}^2 + \bar{z}^2 - e^2}\Big)^{2n-4} \tag{25}$$

is used. It is seen immediately, for the cases $\bar{y}^2 + \bar{z}^2 - e^2 \le 0$, that F becomes singular like $\pi/|\bar{z}|$ and $\pi/2|\bar{z}|$ respectively. However, it can be shown that a similar contribution (of opposite sign) arises from the nonplanar part that exactly cancels this singular term. Thus, the usual practice for planar cases is to evaluate the Mangler principal part of F where these two singularities are cancelled analytically[11].

The incremental nonplanar oscillatory normalwash factor is approximated by

$$D_{2rs} = \frac{\Delta x_s}{8\pi}\int_{-e}^{+e}\frac{Q_2(\bar{\eta})}{[(\bar{y}-\bar{\eta})^2 + \bar{z}^2]^2}d\bar{\eta} \tag{26}$$

where $Q_2(\bar{\eta})$ is another quartic approximation

$$Q_2(\bar{\eta}) = A_2\bar{\eta}^2 + B_2\bar{\eta} + C_2 + D_2\bar{\eta}^3 + E_2\bar{\eta}^4 \approx \{K_2\exp[-i\omega(x_0 - \bar{\eta}\tan\lambda_s)/U] - K_{20}\}T_2^* \tag{27}$$

Letting $Q_2(-e)$, $Q_2(-e/2)$, $Q_2(0)$, $Q_2(e/2)$ and $Q_2(e)$ denote the inboard, inboard intermediate, center, outboard intermediate and outboard values of $Q_2(\bar{\eta})$, respectively, we have

$$A_2 = -\frac{1}{6e^2}[Q_2(-e) - 16Q_2(-e/2) + 30Q_2(0) - 16Q_2(e/2) + Q_2(e)] \tag{28}$$

$$B_2 = \frac{1}{6e}[Q_2(-e) - 8Q_2(-e/2) + 8Q_2(e/2) - Q_2(e)] \tag{29}$$

$$C_2 = Q_2(0) \tag{30}$$

$$D_2 = -\frac{2}{3e^3}[Q_2(-e) - 2Q_2(-e/2) + 2Q_2(e/2) - Q_2(e)] \tag{31}$$

$$E_2 = \frac{2}{3e^4}[Q_2(-e) - 4Q_2(-e/2) + 6Q_2(0) - 4Q_2(e/2) + Q_2(e)] \tag{32}$$

The nonplanar downwash factor is then given by Eq. (33).

$$D_{2rs} = \frac{\Delta x_s}{16\pi\bar{z}^2}\Big\{[(\bar{y}^2+\bar{z}^2)A_2+\bar{y}B_2+C_2+\bar{y}(\bar{y}^2+3\bar{z}^2)D_2+(\bar{y}^4+6\bar{y}^2\bar{z}^2-3\bar{z}^4)E_2]F$$

$$+\frac{1}{(\bar{y}+e)^2+\bar{z}^2}\Big\{[(\bar{y}^2+\bar{z}^2)\bar{y}+(\bar{y}^2-\bar{z}^2)e]A_2+(\bar{y}^2+\bar{z}^2+\bar{y}e)B_2+(\bar{y}+e)C_2$$

$$+[\bar{y}^4-\bar{z}^4+(\bar{y}^2-3\bar{z}^2)\bar{y}e]D_2+[(\bar{y}^4-2\bar{y}^2\bar{z}^2-3\bar{z}^4)\bar{y}+(\bar{y}^4-6\bar{y}^2\bar{z}^2+\bar{z}^4)e]E_2\Big\} \tag{33}$$

$$-\frac{1}{(\bar{y}-e)^2+\bar{z}^2}\Big\{[(\bar{y}^2+\bar{z}^2)\bar{y}-(\bar{y}^2-\bar{z}^2)e]A_2+(\bar{y}^2+\bar{z}^2-\bar{y}e)B_2+(\bar{y}-e)C_2$$

$$+[\bar{y}^4-\bar{z}^4-(\bar{y}^2-3\bar{z}^2)\bar{y}e]D_2+[(\bar{y}^4-2\bar{y}^2\bar{z}^2-3\bar{z}^4)\bar{y}-(\bar{y}^4-6\bar{y}^2\bar{z}^2+\bar{z}^4)e]E_2\Big\}$$

$$+\left[\bar{z}^2\log\frac{(\bar{y}-e)^2+\bar{z}^2}{(\bar{y}+e)^2+\bar{z}^2}\right]D_2+4\bar{z}^2\left[e+\bar{y}\log\frac{(\bar{y}-e)^2+\bar{z}^2}{(\bar{y}+e)^2+\bar{z}^2}\right]E_2\Big\}$$

$$D_{2rs} = \frac{e\Delta x_s}{8\pi(\bar{y}^2+\bar{z}^2-e^2)}\Big\{\frac{1}{[(\bar{y}+e)^2+\bar{z}^2][(\bar{y}-e)^2+\bar{z}^2]}[2(\bar{y}^2+\bar{z}^2+e^2)(e^2A_2+C_2)$$

$$+4\bar{y}e^2B_2+2\bar{y}(\bar{y}^4-2e^2\bar{y}^2+2\bar{y}^2\bar{z}^2+3e^4+2e^2\bar{z}^2+\bar{z}^4)D_2$$

$$+2(3\bar{y}^6-7e^2\bar{y}^4+5\bar{y}^4\bar{z}^2+6e^4\bar{y}^2+6e^2\bar{y}^2\bar{z}^2-3e^2\bar{z}^4-\bar{z}^6+\bar{y}^2\bar{z}^4-2e^4\bar{z}^2)E_2] \tag{34}$$

$$-\frac{(\delta_1\varepsilon+\Delta)}{e^2}[(\bar{y}^2+\bar{z}^2)A_2+\bar{y}B_2+C_2+\bar{y}(\bar{y}^2+3\bar{z}^2)D_2+(\bar{y}^4+6\bar{y}^2\bar{z}^2-3\bar{z}^4)E_2]\Big\}$$

$$+\frac{\Delta x_s}{8\pi}\left\{\frac{D_2}{2}\log\frac{(\bar{y}-e)^2+\bar{z}^2}{(\bar{y}+e)^2+\bar{z}^2}+2\left[e+\bar{y}\log\frac{(\bar{y}-e)^2+\bar{z}^2}{(\bar{y}+e)^2+\bar{z}^2}\right]E_2\right\}$$

where

$$\Delta = \left(\frac{e}{|\bar{z}|}\right)^2\left\{1-\delta_1-\delta_2\frac{\pi}{|\bar{z}|}\left(\frac{\bar{y}^2+\bar{z}^2-e^2}{2e}\right)\right\} \tag{35}$$

The simplification of Eq. (33) via Eq. (22) is tedious but results in the more accurate form above in which ε is again given by Eq. (24). Eq. (34) has been used in general, except when $|(\bar{y}^2+\bar{z}^2-e^2)/2e\bar{z}| \le 0.1$ in which case Eq. (33) is used.

APPLICATIONS

Figures 3, 4 and 5 show the variation of the real part of the incremental kernel numerator along the box quarter-chord for various aspect ratios for a unit Δx rectangular box. The receiving point is on the box itself. The Mach number is M = 0.8 and the reduced frequency is $k_r = 1.0$ based on the box semichord of 0.5. The improved performance of the quartic approximation is evident in the 3 figures and clearly superior with a box aspect ratio of 5.

Four examples are now considered to illustrate the improved convergence characteristics of the quartic approximation. Each example has been investigated in earlier studies. The first three examples are planar: a high aspect ratio rectangular wing, a wing-tail combination, and a wing with a trailing edge control surface. The fourth example is a simplified rectangular T-tail.

A High Aspect Ratio Rectangular Wing. A high aspect ratio, unswept, untapered rectangular wing can be used conveniently to investigate the requirements for box shapes (aspect ratio) and sizes (number of boxes on a chord). At a Mach number of zero, the calculated loads can also be com-

pared to classical two-dimensional solutions if the aspect ratio is high enough, although it should be noted that there are quantitative differences between pressures at cross-sections of a wing with a finite aspect ratio and a two-dimensional airfoil.

An aspect ratio of 20 is selected and the symmetric motion of pitching about the midchord is investigated.

Figures 6 and 7 show the real and imaginary parts, respectively, of the lift due to pitch about the mid-chord. The numbers in the legend (e.g. 10×20) refer to the number of chordwise and spanwise boxes, respectively. The results show that the quartic solution with 20 spanwise strips is closer to the converged solution than the parabolic solution with 40 spanwise strips. In fact, the quartic solution with 10 spanwise boxes has acceptable accuracy up to a reduced frequency of 3.

Figures 8 and 9 show the effect of box aspect ratio on convergence for the same wing. Additional cases were calculated with 5 chordwise boxes. The real part converges more slowly than the imaginary part, however, the quartic is closer to convergence with far fewer boxes than the parabolic approximation. The immediate implications of this are that existing models are accurate to a higher reduced frequency without any change. Conversely, smaller models can be generated to give the same accuracy as the parabolic approximation.

The Wing/Horizontal-Stabilizer Combination. This configuration is one of those selected by the AGARD Structures and Materials Panel for comparison of methods used in interfering lifting surface theories. The planar configuration is shown in Fig. 10 with its span divided into 12 strips. The convergence characteristics of the original DLM were studied on this configuration by Rodden, Giesing, and Kalman[6] with a number of different chordwise box divisions on the wing and the tail. The equal chordwise fraction of boxes on the wing and tail, respectively, were 5 and 4, 6 and 5, 10 and 8, and 12 and 10.

The 12 spanwise strips were the same for all combinations of boxes, so the total number of boxes in the various idealizations were 108, 132, 168, 216, and 264. The lift coefficient for oscillatory plunging was obtained at a Mach number of 0.8 and a reduced frequency of $k = \omega s/V = 1.5$ where s is the semispan (based on $b_r = 0.8$, $k_r = 1.2$), and the results are shown in Table 1†. The new results with the quartic approximation have been added to Table 1 for an idealization with the same number of chordwise boxes but with only eight spanwise strips (with divisions at 0.0, 0.1667, 0.3333, 0.5, 0.6667, 0.8333, 0.9, 0.96, and 1.0 fractions of the span), leading to a total number of boxes of 72, 88, 112, 144, and 176 for the different chordwise divisions. A perusal of Table 1 shows the quartic approximation with fewer spanwise strips to have the same accuracy as the earlier parabolic approximation. The convergence of both sets of results with increasing number of chordwise boxes shows the importance of a sufficient number of chordwise boxes per wavelength, 12 as suggested in the published guidelines[8]. The performance of the quartic approximation in this example suggests an increase in the guideline box aspect ratio limit of 3, established for the parabolic approximation, to perhaps 5 for the quartic approximation.

Table 1: Comparison of Lift Coefficients for Plunging, $(C_L/ik(h/s))$ - k_r=1.2, M=0.8

Boxes[a]	Ref. (6)	Boxes[b]	Present Study
108	3.792+i2.955	72	3.751 + i2.932
132	3.961+i2.963	88	3.913 + i2.928
168	4.160+i2.974	112	4.098 + i2.952
216	4.299+i2.960	144	4.251 + i2.966
264	4.359+i2.955	176	4.341 + i2.969

a. 12 Spanwise strips
b. 8 Spanwise strips

The Wing-Aileron Configuration. This configuration is one of those selected by the AGARD Structures and Materials Panel for comparison of methods used in isolated lifting surface theories. The swept-back configuration is Planform No. 2 in Woodcock[12] with the inboard end of the aileron selected at 50% of the wing semispan and is shown in Fig. 11. Two antisymmetric motions are considered: wing in roll and aileron deflection. The AGARD example Mach number of 0.7806 is assumed along with a reduced frequency of 1.0, again based on the wing semispan. Several box idealizations are considered. The wing is divided into three panels: one for the wing inboard of the aileron, one for the wing forward of the aileron, and one for the aileron itself. Three sets of equal chordwise divisions of the inboard wing, the outboard wing, and the aileron are chosen as follows: the number of chordwise boxes in each region are 8, 6, and 2 in the first set, the second set has 12, 9, and 3, and the third set has 16, 12, and 4. Two sets of spanwise divisions are also chosen: the first set has five equal width strips for the inboard wing, and six equal width strips for the outboard wing/aileron region, the second set of spanwise divisions has six equal width strips across the span. With 11 strips, the various chordwise divisions lead to a total of 88, 132, and 176 boxes. With the six strips, the total number of boxes is

† The values labeled Ref. (6) have been recalculated using slightly different strip widths scaled from Fig. 2 of Ref. (6); the actual widths were not reported other than in the figure shown.

48, 72, and 96.

The results in Tables 2 and 3 are rather surprising in that they all indicate convergence of the different aerodynamic models. Further study of this configuration is needed at higher reduced frequencies.

Table 2: Aileron Effectiveness for AGARD Wing/Aileron at M = 0.7806 and k_r=1.0

Boxes	Ref. (6)	Present Study
88	0.3341+i0.1740	0.3334+i0.1743
132	0.3389+i0.1770	0.3395+i0.1770
176	0.3411+i0.1789	0.3425+i0.1784
48	0.3514+i0.1805	0.3536+i0.1788
72	0.3559+i0.1847	0.3595+i0.1822
96	0.3582+i0.1869	0.3621+i0.1842

Table 3: Damping in Roll for AGARD Wing/Aileron at M = 0.7806 and k_r=1.0

Boxes	Ref. (6)	Present Study
88	0.07514-i0.1800	0.07538-i0.1794
132	0.07543-i0.1807	0.07574-i0.1810
176	0.07552-i0.1809	0.07589-i0.1810
48	0.07454-i0.1915	0.07466-i0.1906
72	0.07477-i0.1908	0.07516-i0.1914
96	0.07485-i0.1910	0.07524-i0.1917

The Rectangular T-Tail . The rectangular T-tail that was tested by Clevenson and Leadbetter[13] has also been the subject of previous studies. The wind tunnel tests were performed at low speed and the model was oscillated about the fin mid-chord as shown in Fig. 12. The lattice idealization in the earlier study[6] is also shown in the figure. The present study uses equal rectangular boxes chordwise and equal spanwise on the vertical tail and equal boxes chordwise on the horizontal tail. The spanwise variation in fraction of semispan is (0.0, 0.05, 0.17, 0.3, 0.4, 0.5, 0.6, 0.7, 0.8, 0.9, 1.0), with the spacing at the inboard edge to give similar strip widths on the vertical and horizontal tail at the intersection. The earlier study[6] and the experiment[13] both nondimensionalized the coefficients in non-standard ways. The present study uses a reference semichord of $b_r = c/2 = 0.5$ ft, fin area to normalize the forces and fin span to normalize the moments. Figures 13, 14 and 15 show the variation with reduced frequency of the magnitude and phase angle of the side force, yawing moment and rolling moment (about an axis 0.5 ft below the base of the fin), due to oscillatory rigid body yawing of the fin about its midchord. The quartic approximation gives the same results as the original study[6] for these low reduced frequencies. Figures 16, 17 and 18 show that a reduction in the number of spanwise strips from 10 to 5 shows the quartic approximation to have the same accuracy as the earlier study[6].

CONCLUDING REMARKS

A refinement to the Doublet-Lattice subsonic lifting surface method has been formulated and implemented. The quartic approximation to the kernel function allows either an increase in accuracy for current box schemes, or a reduction in the number of boxes (and subsequently the storage requirements) for the same accuracy. From the results presented, the limit on box aspect ratio (formerly 3 with the original method) can now be relaxed to 5. This also allows a little more flexibility in modelling, as boxes tend to have a higher aspect ratio normally towards the tips of tapered wing aircraft.

The present study has only considered rigid body modes at a small number of Mach numbers and reduced frequencies. Further analyses are needed to establish more accurately the maximum value of box aspect ratio, tentatively proposed at 5. Another guideline is also needed since a minimum number of spanwise strips has never been established for the previous DLM. This would be a function of the aspect ratio of the lifting surface and its vibration modeshapes, i.e., the number of node lines across the span. Further studies are planned on more practical configurations and the convergence characteristics of the new DLM will be investigated in future flutter and gust response analyses.

APPENDIX A

QUADRATURE ROUTINE FOR INTEGRALS IN THE LIFTING LINE ELEMENT METHOD

by
Valter J. E. Stark†

The Doublet-Lattice Method (DLM)[1] and the independently developed Lifting Line Element Method[2] (LLEM) were presented for the first time at the same AIAA Meeting in New York City in 1968. Some practical applications of the LLEM were shown, but the method was not described in detail.

† Consultant, AERELCO, Linköping 587 39, Sweden

The two methods are in principle identical, but there is a difference as regards the treatment of certain integrals on the lifting line elements. The routine applied in the LLEM shall be described here.

The relation between the y- and z-components of the dimensionless velocity and the dimensionless pressure jump $\Delta p(u,v)$ across the lifting-surface S may be written

$$(\phi_y,\phi_z) = -\iint_S \Delta p(u,v)\left(\frac{\partial}{\partial y},\frac{\partial}{\partial z}\right)\frac{\partial I}{\partial z}\frac{dudv}{8\pi} \tag{A.1}$$

$$= \iint_S \Delta p(u,v)(-(y-v)zr^2 I_{rr} + (y-v)zrI_r + z^2r^2 I_{rr} + (y-v)^2 rI_r)\frac{dudv}{r^4 8\pi} \tag{A.2}$$

where $I_r = \frac{\partial I}{\partial r}$, $I_{rr} = \frac{\partial I_r}{\partial r}$

$$I = e^{i\omega(u-x)}\int_\tau^\infty (t^2+r^2)^{-0.5} e^{-i\omega t}dt$$

$$\tau = (u - x + MR)/B$$

$$R = \sqrt{(u-x)^2 + Br^2}$$

$$r = \sqrt{(y-v)^2 + z^2}$$

$$B = 1 - M^2$$

with M and ω being the Mach number and the reduced frequency, respectively.

By using a second imaginary unit $j = \sqrt{-1}$ for separation of the velocity components and for definition of the complex variable Z = y + jz, we may write Eq. (A.2) in a more compact form

$$\phi_y - j\phi_z = \iint_S \Delta p(u,v)\left(j\frac{\partial}{\partial Z}\left(\frac{1}{Z-v}\right)F + \frac{1}{Z-v}\frac{z}{r^2}G\right)\frac{dudv}{8\pi} \tag{A.3}$$

where

$$F = rI_r$$

$$G = rI_r + r^2 I_{rr}$$

The integral relation (A.3), as well as the corresponding relation in the DLM, is reduced to a set of linear equations by introducing a number of lifting-lines

$$x = X_m(y) \tag{A.4}$$

(for ms lifting lines, the m^{th} line was located at the fractional chord [0.25+m-1]/ms), a number of strips bounded by chords

$$y = y_n \pm d_n \tag{A.5}$$

(for ns chords, the n^{th} chord was located at the fractional span [2(n-1)+1]/(4ns+1)) and the expression

$$\sum_{m,n} P_{m,n}\Delta(u - X_m(v),(v-y_n)/d_n) \tag{A.6}$$

where $P_{m,n}$ is an undetermined constant, $\Delta(\ ,\ )$ is a special function defined by

$$\Delta(x,\eta) = \begin{cases}\delta(x) & \text{for } |\eta| < 1 \\ 0 & \text{for } |\eta| > 1\end{cases} \tag{A.7}$$

and $\delta(x)$ is the Dirac delta function. Inserting the expression (A.6) for $\Delta p(u,v)$ in Eq. (A.3) yields

$$\phi_y - j\phi_z = \sum_{m,n} W_{m,n}(x,y,z)P_{m,n} \tag{A.8}$$

where

$$W_{m,n}(x,y,z) = \int_{-1}^{1}\left(j\frac{\partial}{\partial Z}\left(\frac{1}{Z-v}\right)F + \frac{1}{Z-v}\frac{z}{r^2}G\right)\frac{dv}{8\pi} \tag{A.9}$$

Since ϕ_y and ϕ_z, for a given mode of oscillation are given, equations for determining $P_{m,n}$ can be obtained by requiring that the two members of Eq. (A.8) shall be equal at chosen control points (x,y,z) on the lifting surfaces.

The elements of the matrix of these equations are given by the integral (A.9). A change of the integration variable yields

$$W_{m,n}(x,y,z) = \int_{-1}^{1}\left(j\frac{\partial}{\partial\zeta}\left(\frac{1}{\zeta-\eta}\right)\frac{F}{d_n^2} + \frac{1}{\zeta-\eta}\frac{zG}{d_n r^2}\right)\frac{d\eta}{8\pi} \tag{A.10}$$

where

$$\zeta = (y - y_n + jz)/d_n$$

F and G are defined as in Eq. (A.3)

$$I = e^{i\omega(U_m - x)}\int_\tau^\infty (t^2+r^2)^{-0.5} e^{-i\omega t}dt$$

$$U_m = X_m(y_n + \eta d_n)$$

$$\tau = (U_m - x + MR)/B$$

$$R = \sqrt{(U_m - x)^2 + Br^2}$$

$$r = \sqrt{(y - y_n - \eta d_n)^2 + z^2}$$

In the LLEM, the integral (A.10) was calculated by Fourier expansion of F/d_n^2 and $zG/d_n r^2$ in terms of Legendre

polynomials $P_\nu(\eta)$. The coefficients of the expansions, denoted by a_ν and b_ν, respectively, were obtained from

$$(a_\nu, b_\nu) = \frac{2\nu+1}{2}\int_{-1}^{1}\left(\frac{F}{d_n^2}, \frac{zG}{d_n r^2}\right)P_\nu(\eta)d\eta \qquad (A.11)$$

by numerical Gaussian quadrature. Using the expansions for evaluating the integral (A.10), we find

$$W_{m,n}(x,y,z) = \sum_\nu\left(a_\nu\frac{\partial}{\partial\zeta}Q_\nu(\zeta) + b_\nu Q_\nu(\zeta)\right)\frac{1}{4\pi} \qquad (A.12)$$

where $Q_\nu(\zeta)$ is the Legendre polynomial of the second kind and order ν, which is related to $P_\nu(\eta)$ through

$$Q_\nu(\zeta) = \frac{1}{2}\int_{-1}^{1}\frac{P(t)}{\zeta - t}dt \qquad (A.13)$$

Formulas for $Q_\nu(\zeta)$ can be found in Jahnke and Emde[14].

The Fourier expansions described above and employed in the LLEM seem favorable, because an attempt to increase the accuracy by increasing the number of terms in the expansion only implies calculation of a few more coefficients and then using a few more integration points for evaluating the integral (A.11).

As there was no time in the sixties for determining the number of terms required for the desired accuracy, the applications described in Landahl and Stark[2] were simply performed by retaining only three terms containing P_0, P_1, and P_2. The resulting approximations were thus polynomials of degree 2 as in the earlier version of the DLM. The two methods were thus expected to yield not identical but closely agreeing results.

The Fortran program developed (by a research agency separate from SAAB) was found to be very expensive to run on the computers available in the mid-sixties, and this led to the decision to try other approaches[15].

APPENDIX B

Two integrals are involved in the evaluation of the kernel function that have utilized approximations to the function $1 - u/\sqrt{(1+u^2)}$. The original work[1] used an approximation developed by Watkins, Woolston and Cunningham[16] and later work[17] used a more accurate approximation of Laschka[18]. The comparisons in the present paper are based on the approximation of Laschka.

An improved approximation developed by Desmarais[19] will be used in subsequent studies. This approximation has the form:

$$1 - u/\sqrt{(1+u^2)} = \sum_{k=1}^{n} a_k \exp[-(2^{k/m})bu] \qquad (B.1)$$

and Desmarais has obtained the coefficients b and a_k corresponding to various values of m and n for n varying from 8 to 72. The twelve term approximation D12.1 has been used here and its parameters are tabulated below.

Table B.1: Approximation D12.1

n=12	m=1	b=.009054814793
a_1		.000319759140
a_2		-.000055461471
a_3		.002726074362
a_4		.005749551566
a_5		.031455895072
a_6		.106031126212
a_7		.406838011567
a_8		.798112357155
a_9		-.417749229098
a_{10}		.077480713894
a_{11}		-.012677284771
a_{12}		.001787032960

A comparison of some generalized forces using the Laschka and Desmarais D12.1 approximations is shown in Table B.2 for the Wing/Horizontal Stabilizer configuration. The differences here are seen to be small and their effect on flutter speeds will be the subject of a later investigation.

A computer program now called N5KQ incorporates the quartic feature of this paper and the Desmarais D12.1 approximation, and is available from the authors.

Table B.2: Comparison of Generalized Forces for Plunging, (C_L/ik(h/s)) - k_r=1.2, M=0.8

No. of Boxes	Ref. (6)	D12.1
108	3.792+i2.955	3.770+i2.965
132	3.961+i2.963	3.938+i2.974
168	4.160+i2.974	4.136+i2.986
216	4.299+i2.960	4.274+i2.973
264	4.359+i2.955	4.333+i2.969

REFERENCES

1 Albano, E., and Rodden, W. P., "A Doublet–Lattice Method for Calculating Lift Distributions on Oscillating Surfaces in Subsonic Flows", *AIAA J.*, Vol. 7, pp. 279-285, p. 2192, 1969.

2 Landahl, M. T., and Stark, V. J. E., "Numerical Lifting-Surface Theory - Problems and Progress", *AIAA J.*, Vol. 6, pp. 2049-2060, 1968.

3 Wittmeyer, H., "Aeroelastomechanische Untersuchungen an dem Flugzeug SAAB 37'Viggen'", Jahrbuch 1968, pp 11-23, Ludwig Prandtl-Gedächtnis Vorlesung, München.

4 Vivian, H. T., and Andrew, L. V., Unsteady Aerodynamics for Advanced Configurations: Part I - Application of the Subsonic Kernel Function to Nonplanar Lifting Surfaces, Air Force Flight Dynamics Laboratory, Report FDL–TDR–64–152, 1965.

5 Landahl, M. T., "Kernel Function for Nonplanar Oscillating Surfaces in a Subsonic Flow", *AIAA J.*, Vol. 5, pp. 1045-1046, 1967.

6 Rodden, W. P., Giesing, J. P., and Kalman, T. P., "Refinement of the Nonplanar Aspects of the Subsonic Doublet–Lattice Lifting Surface Method", *J. Aircraft*, Vol. 9, pp. 69-73, 1972.

7 Hedman, S. G., "Vortex Lattice Method for Calculation of Quasi Steady State Loadings on Thin Elastic Wings". Aeronautical Research Institute of Sweden, Report 105, 1967.

8 Rodden, W. P., and Johnson, E. H., "*MSC/NASTRAN Aeroelastic Analysis User's Guide*", The MacNeal–Schwendler Corporation, 1994.

9 Anon., Federal Aviation Regulations - Part 25 - Airworthiness Standards: Transport Category Airplanes, Department of Transportation, Federal Aviation Administration, Washington DC.

10 Anon., Joint Airworthiness Requirements - JAR 25, Large Airplanes, Civil Aviation Authority, Cheltenham, UK.

11 Mangler, K. W., "Improper Integrals in Theoretical Aerodynamics", Royal Aircraft Establishment, Report Aero 2424, C.P. No. 94, 1951.

12 Woodcock, D. L., "A Comparison of Methods Used in Lifting Surface Theory", AGARD Report No. 583, Supplement to the AGARD Manual on Aeroelasticity, Part VI, 1971.

13 Clevenson, S. A., and Leadbetter, S. A., "Measurements of Aerodynamic Forces and Moments at Subsonic Speeds on a Simplified T-Tail Oscillating in Yaw About The Fin Midchord", TN 4402, 1958, NACA.

14 Jahnke, E., and Emde, F., "Tables of Functions With Formulae and Curves", New York: Dover, 1945, p.107.

15 Stark, V. J. E., "The AEREL Flutter Prediction System", ICAS Paper 90-1.2.3, September 1990.

16 Watkins, C. E., Woolston, D. S., and Cunningham, H. J., "A Systematic Kernel Function Program for Determining Aerodynamic Forces on Oscillating or Steady Finite Wings at Subsonic Speeds", R-48, 1959, NASA.

17 Kalman, T. P., Rodden, W. P., and Giesing, J. P., "Application of the Doublet-Lattice Method to Nonplanar Configurations in Subsonic Flow", *J. Aircraft*, Vol. 8, No. 6, 1971, pp. 406-413.

18 Laschka, B. "Zur Theorie der harmonisch schwingenden tragenden Fläch bei Unterschallanströmung",*Zeitschrift für Flugwissenschaften,* Vol. 11, No. 7, 1963, pp. 265-292.

19 Desmarais, R.N., "An Accurate Method for Evaluating the Kernel of the Integral Equation Relating Lift to Downwash in Unsteady Potential Flow". AIAA Paper No. 82-687, presented at the AIAA/ASME/ASCE/AHS 23rd Structures, Structural Dynamics and Materials Conference, New Orleans, LA, 1982.

FIGURES & TABLES

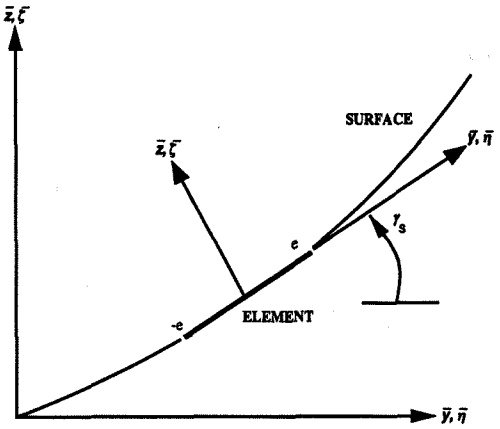

Fig. 1: Lifting Surface Coordinate System

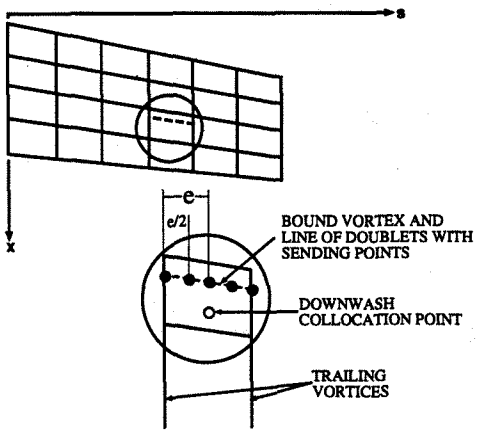

Fig. 2: Idealization of Lifting Surface using trapezoidal boxes

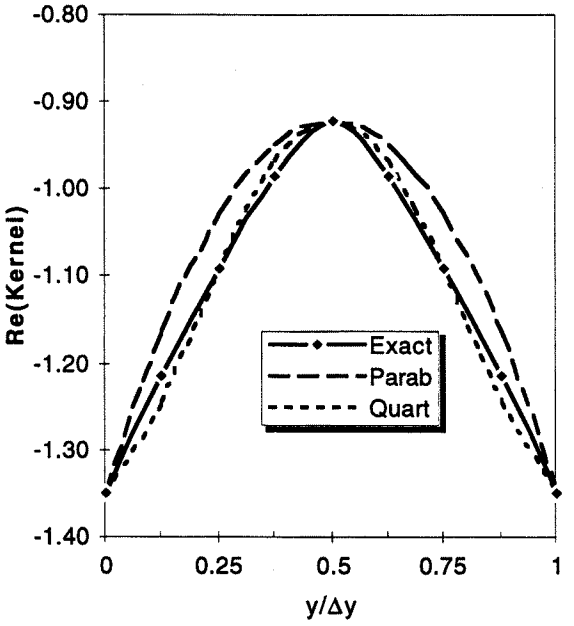

Fig. 3: Variation of Incremental Kernel Along Box Quarter-Chord, AR = 1.0

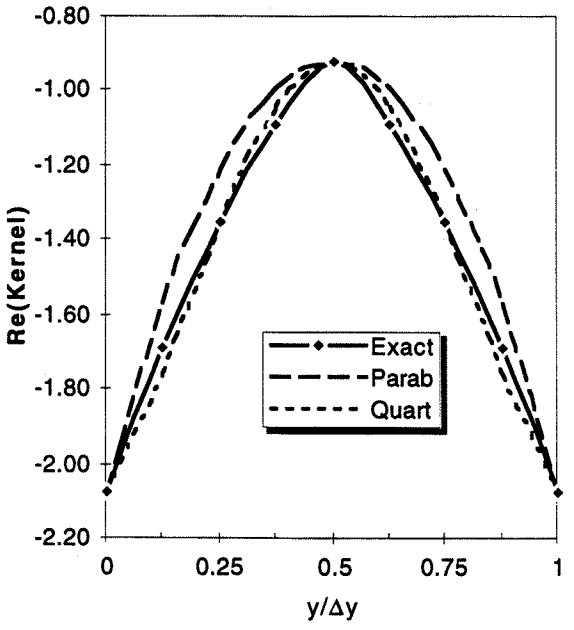

Fig. 4: Variation of Incremental Kernel Along Box Quarter-Chord, AR = 2.0

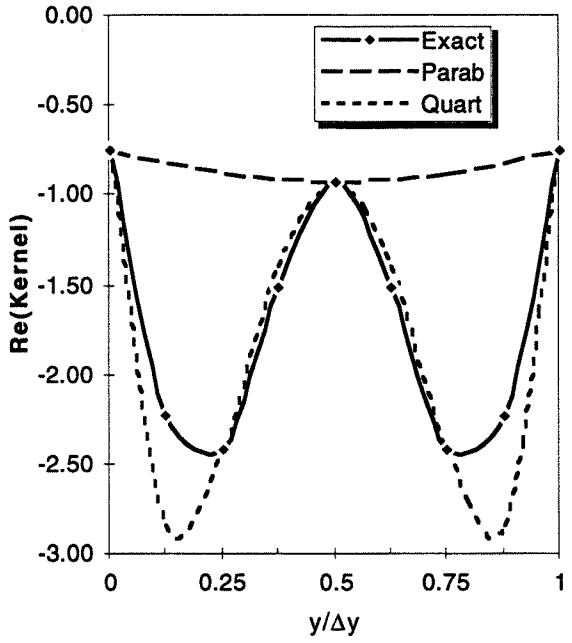

Fig. 5: Variation of Incremental Kernel Along Box Quarter-Chord, AR = 5.0

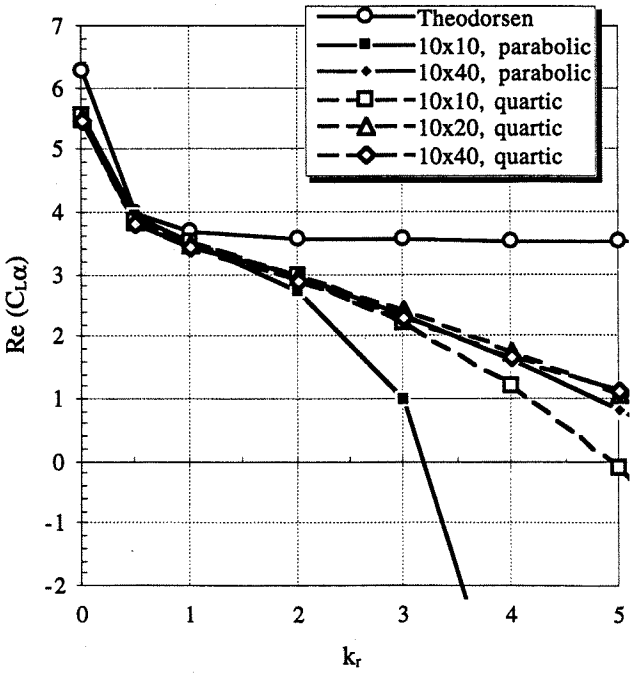

Fig. 6: Re($C_{L\alpha}$) vs k_r, AR=20 Wing, Mach=0.0

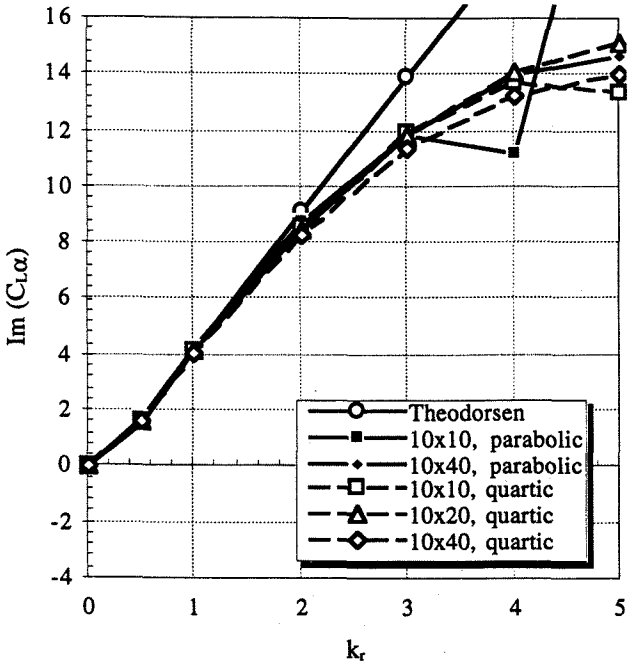

Fig. 7: Im($C_{L\alpha}$) vs k_r, AR=20 Wing, Mach=0.0

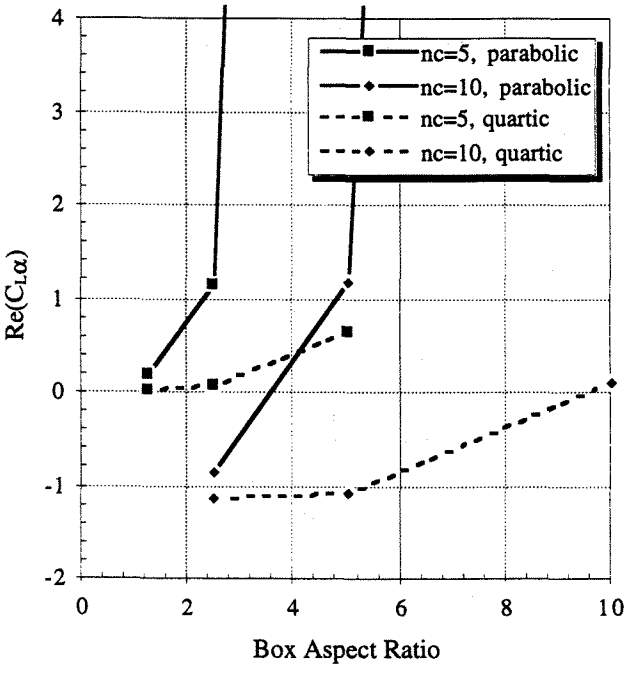

Fig. 8: Effect of Box Aspect Ratio on Convergence, AR = 20 Wing, Mach=0.0, k_r=5.0

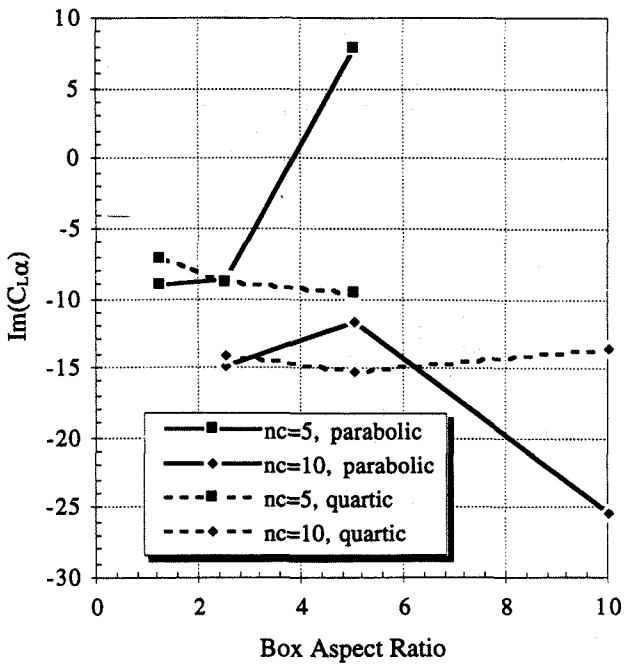

Fig. 9: Effect of Box Aspect Ratio on Convergence, AR = 20 Wing, Mach=0.0, k_r=5.0

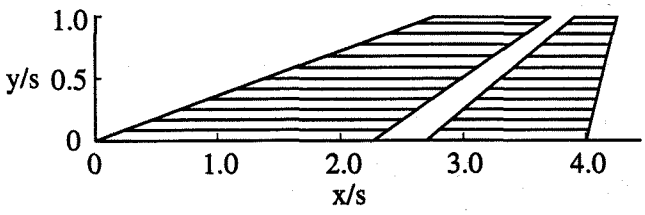

Fig. 10: Wing/Horizontal Tail Configuration

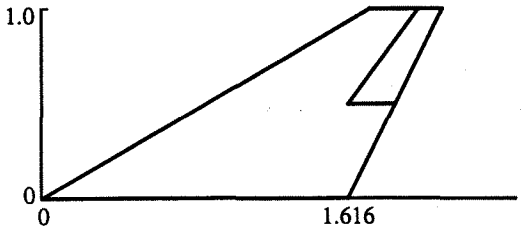

Fig. 11: Wing-Aileron Configuration

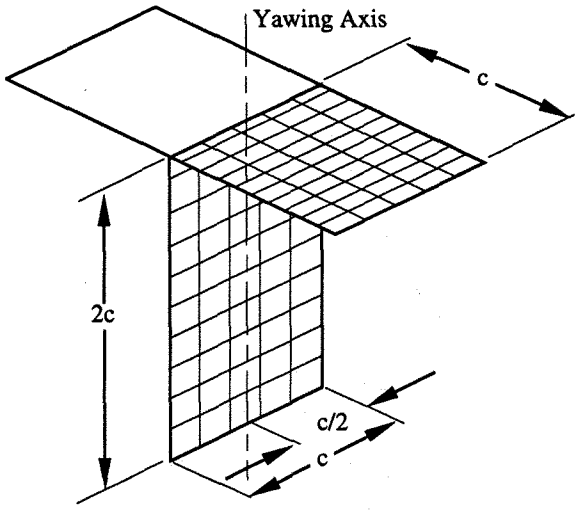

Fig. 12: Rectangular T-Tail Configuration

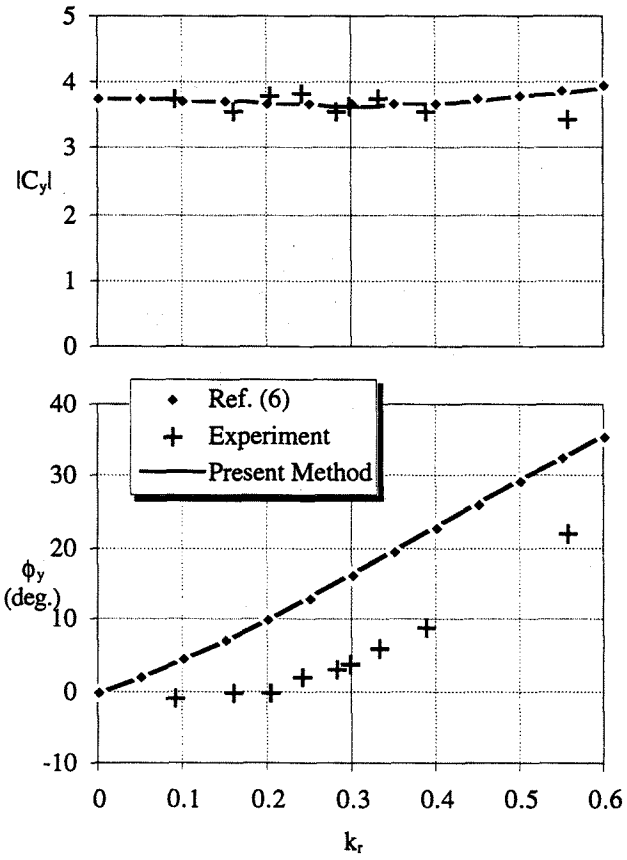

Fig. 13: Side Force Coefficient vs. k_r for T-Tail

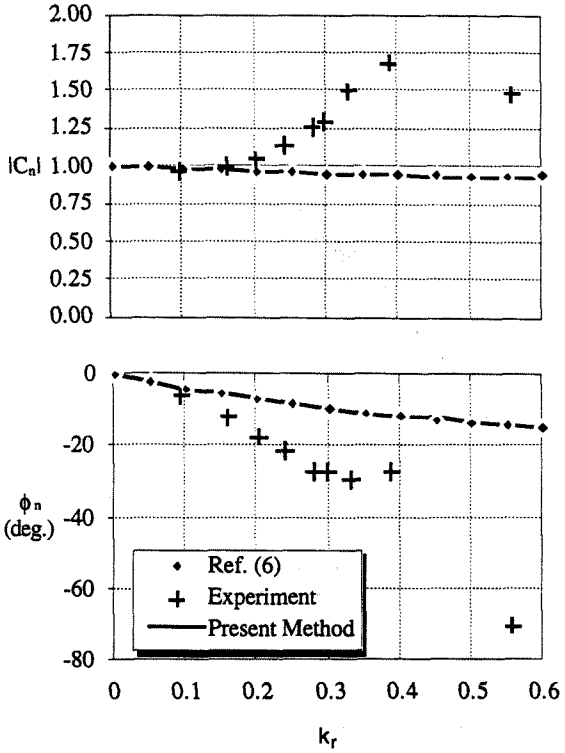

Fig. 14: Yawing Moment Coefficient vs. k_r for T-Tail

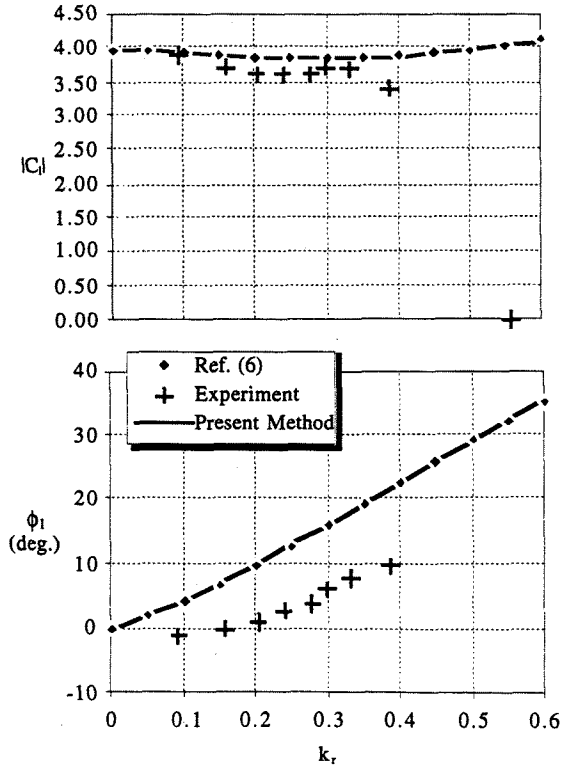

Fig. 15: Rolling Moment Coefficient vs. k_r for T-Tail

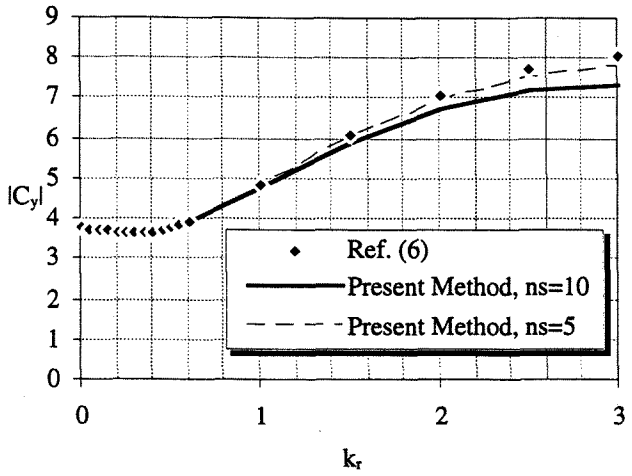

Fig. 16: Effect of no. spanwise boxes on C_y, T-Tail

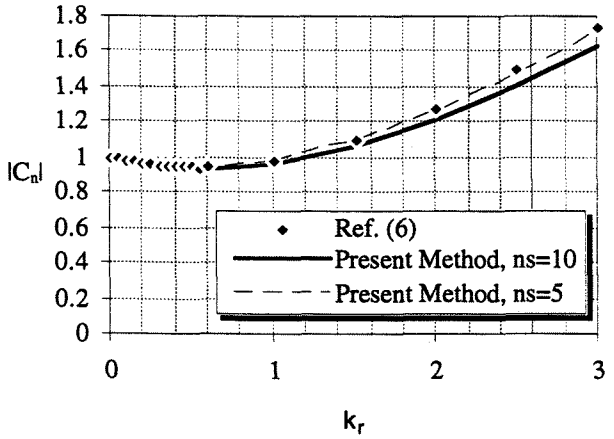

Fig. 17: Effect of no. spanwise boxes on C_n, T-Tail

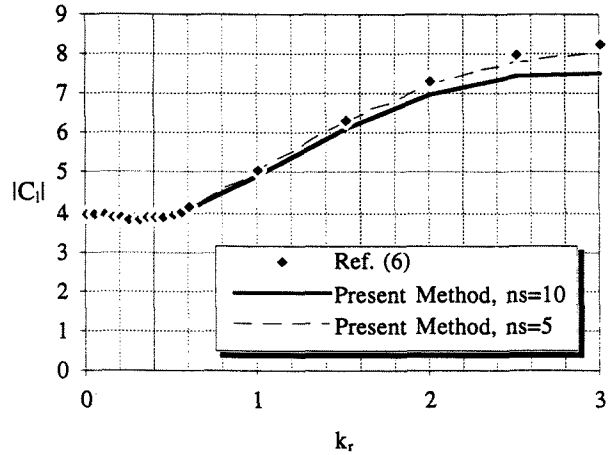

Fig. 18: Effect of no. spanwise boxes on C_l, T-Tail